Optimization of the Acid blue 113 dye degradation in the three-dimensional electro persulfate process (3D/EPS) catalyzed by granular activated carbon (GAC) using the response surface methodology

Alireza Rahmani[a], Abdolmotaleb Seid-Mohammadi[b], Mohammad Khazaei[b], Somayeh Maroofi[c]*

[a]*Department of Environmental Health Engineering, School of Public Health, Hamadan University of Medical Sciences, Hamadan, Iran, email: rahmani@umsha.ac.ir (A. Rahmani)*
[b]*Social Determinants of Health Research Center (SDHRC), Environmental Health Engineering, School of Public Health, Hamadan University of Medical Sciences, Hamadan, Iran, emails: sidmohammadi@umsha.ac.ir (A. Seid-Mohammadi), khazaei57@gmail.com (M. Khazaei)*
[c]*M.Sc of Environmental Health Engineering, School of Public Health, Hamadan University of Medical Sciences, Hamadan, Iran, Tel. +989186067993; email: somayemaroofi2019@gmail.com (S. Maroofi)*

ABSTRACT

In this experimental study, the effect of five important independent variables, for example, solution pH, persulfate concentration, electrode potential, granular activated carbon (GAC) mass, and retention time on the removal efficiency of acid blue 113 (AB113) dye in 3D/EPS (electro persulfate process) process was evaluated and optimized using response surface methodology along with the central composite design. All electrochemical reactions were performed in a Plexiglass reactor (with a useful volume of 250 mL) equipped with graphite anode and stainless steel cathode electrodes and activated carbon as the third electrode (Third dimension). According to the results of the analysis of variance ($P > F$-value <0.0001) and Fit statistic (R_{adj}^2 = 0.9953), the proposed quadratic model for removal of AB113 had suitable adequacy and accuracy. The optimum conditions for dye removal, with maximum efficiency of 90.51%, were pH of 5.50, persulfate concentration of 22.59 mM, the electrode potential of 15 V, the retention time of 24.99 min, and GAC of 12.5 g. The dye removal efficiencies through the application of persulfate, electrochemical, and 2D electro persulfate processes under the same conditions were obtained to be 5.4%, 42.6%, and 70.25%, respectively. The results of scanning electron microscopy and X-ray diffraction analyses of the surface of activated carbon after the reaction show that intermediate compounds produced can be retained on the porous surface and increase the dye removal efficiency. The most important intermediates produced, with the lowest molecular mass, were oxalic acid ($C_2H_2O_4$), malonic acid ($C_3H_4O_4$), naphthalene-1, and 4-diamine ($C_{10}H_{10}N_2$). According to the results, the rate of total organic carbon reduction was 85% at the end of 75 min. According to the obtained results, this process, in a short time, can be considered as an advanced electrochemical oxidation method. It can also be used for the treatment of colored wastewater such as textile wastewater.

Keywords: Acid Blue 113 dye; 3D electro persulfate process; Optimization; Response surface methodology

1. Introduction

The increasing population growth and the expansion of industry and agriculture have caused the shortage of safe water in the world. Therefore, treatment and reuse of consumed water have found especial importance [1]. Water pollution by synthetic dyes is very important due to the production and use of different dyes throughout the world [2]. Many industries such as cosmetics, leather, printing, and textile industries produce colorful effluents [3]. Textile

* Corresponding author.

wastewaters, which are containing synthetic dyes, are of the most important sources of water pollution [4]. The residual dye solution in water may contain biological contaminants that halt photosynthetic activity in aquatic life. The presence of dye in the water is led to the unsuitability of the water for consumption [5]. At present, worldwide production of dyes exceeds 7×10^5 tons per year [6], which 2.8×10^5 tons is discharged from industrial effluent [7]. There are three categories of dyes used in the textile industry, which include anionic (direct, acid, and reactive dyes), cationic (primary dyes), non-ionic (dispersive dyes) [8]. Among all types of commercial synthetic dyes, azo dyes are the largest group of dyes representing a wide range of colors and structures [9]. Azo dyes are characterized by azo groups containing one or more nitrogen-nitrogen double bonds (N=N) [10]. The dye used in this study is AB 113, an acidic dye, which belongs to the anionic group [11]. It is known as a diazo dye, which has two azo groups in its chemical structure and is soluble in water and is widely used in the textile industries for dyeing the wool and Silk and in manufacturing the leather and paper [12–14]. Acidic dyes are generally used for polyamide, wool, silk, modified acrylic, and polypropylene fibers, as well as blended fibers such as cotton, rayon, polyester, and ordinary acrylic. Usually, 80%–85% of the acid dyes used in the United States (US) textile industries are employed for dyeing nylon and 15%–20% of them are used for dyeing wool [15]. Discharging the dye-containing effluents from industries releases toxic, mutagenic, and carcinogenic and allergenic products [4,16], which are harmful to human and living organisms [17] and cause aesthetic problems in water resources [18]. Most of these dyes cause jaundice, tumor progression, skin irritation, allergies, heart defects [19], and severe kidney and nervous system damages in humans [20]. In general, they are harmful to water and are toxic to the environment [21]. Thus, the removal of dyes from wastewater has become an important environmental subject [22]. Today, several physicochemical processes, including adsorption, coagulation, flocculation, sedimentation, ion exchange, foam floatation, membrane separation, electrochemical [23–25], catalytic degradation [26], and photocatalysts have been used to remove dyes from aqueous media [27]. Since most conventional physical and chemical treatment methods are unable to remove dye compounds [28], the use of advanced oxidation processes to remove such toxic and resistant organic compounds has been considered by researchers and operators of water and wastewater treatment plants [29–31], which the basis of these methods is the production of strong oxidizing species such as sulfate and hydroxyl radicals. Sulfate radicals have a longer half-life (10–20 d) compared to hydroxyl radicals, and its potential in the treatment of wastewater has been proven [32]. Sodium persulfate is the newest oxidant introduced with the potential oxidation of 2.01 V. Its advantages are including cheapness, non-selective oxidation of organic compounds, high stability of produced radicals under different conditions, high solubility, having solid form, and thus ease of transport and storage [33,34]. To produce the sulfate radical and to use it as an advanced oxidation process, the persulfate anion must be activated. Activation of persulfate has been performed by heat [35], ultraviolet light [36], ultrasound [37], transition metal (Me^{2+}) [38], and other methods [39–42]. The final product of activation is the production

of persulfate radical with an oxidation potential of 2.6 eV [34]. Recently, the use of electric current for the activation of persulfate has been considered as a clean and simple method which is performed by an electron. Reaction 1 illustrates this process. An important advantage of this method, compared to other activation methods, is the use of the synergistic effect of the enhanced electrochemical oxidation process along with oxidation by persulfate [43].

$$S_2O_8^{2-} + 2e \rightarrow SO_4^{\bullet-} + SO_4^{2-} \qquad (1)$$

Two-dimensional or conventional electrochemical processes have limitations such as mass transfer, low surface-to-volume ratio, increased energy consumption, the short lifetime of electrode materials, increasing the temperature during the process, and low process efficiency in industrial applications. These limitations can be reduced by the use of the three-dimensional electro persulfate process (3D/EPS) catalyzed by granular activated carbon (GAC). The removal of target pollutants using the 3D/EPS process is much higher because of the specific surface area, and therefore electrons and active sites are much higher than two-dimensional types [44].

The results showed that this system has an excellent capacity for reducing pollutants and dyes, as well as improving biodegradability by producing more H_2O_2 and OH [45]. Investigation of effective parameters in engineering studies using the One-factor-at-a-time (OFAT) method is to study the processes that have several variables and responses and require a large number of experiments, which in addition to increasing project execution costs, it will also increase the project execution time. Moreover, in this statistical method, the optimization of the parameters involved in the study will not be possible due to the lack of consideration of the interactions between the parameters and the system response [46].

In this study, the effect of independent parameters on process response as well as optimization of parameters was investigated using response surface methodology based on the central composite design (RSM-CCD) [47]. Compared to the OFAT method, the RSM-CCD method is able to forecast the individual, interaction, and quadratic effects between parameters and response and, finally, to predict the process response by developing a quadratic mathematical model. The ability to find the optimum point outside the tested points with accuracy equal to the tested points is another advantage of this statistical method [48].

Therefore, due to the presence of dyes as the main pollutants in water and considering the special advantages and features of 3D advanced oxidation processes (AOPs) in the removal of organic compounds, especially dyes, the present study was carried out to evaluate the efficiency of 3D/EPS process with GAC catalyst.

2. Materials and methods

2.1. Chemicals and reagents

Sodium persulphate (purity of 98%), sulfuric acid, and sodium hydroxide were provided from Sigma Aldrich (St. Louis, MO, USA). GAC with a size of 1.5 mm and

graphite and stainless steel (SS) electrodes were obtained from Kimia Gostar Poyesh Co., Iran. Acid Blue 113 (AB113) was prepared by Alvan Sabet Co., Hamadan. The general characteristics of Acid Blue 113 are shown in Table 1. 0.1 N sulfuric acid (H_2SO_4) and 0.1 N sodium hydroxide (NaOH) were applied to regulate the pH of the solutions [HACH model sension1 (USA)]. Double distilled water was utilized to prepare the solutions. All the chemicals used in the experiments were of analytical grade and were applied without further purification.

2.2. Analytical procedure

After conducting the related experiments, the samples were collected at predetermined time intervals and were filtered through a 0.45 μm membrane filter, and the concentration of AB113 dye was finally measured using an ultraviolet-visible spectrophotometer (DR5000) at a wavelength of 567 nm [49]. To select this wavelength, a certain concentration of dye was prepared at pH 7. Then, the wavelength scan was performed at 200–700 nm using a quartz cell and DR 5000 spectrophotometer. The desired peak was obtained at 567 nm. The concentration-absorption standard curve was plotted and used to convert the absorbance values to the concentration in mg/L.

The efficiency of the 3D/EPS catalyzed by the GAC process in removing AB113 dye was calculated using Eq. (2) and the removal efficiency of total organic carbon (TOC) by this process was determined using Eq. (3).

$$AB\ 113\ Removal\ (\%) = \frac{\left[AB\ 113\right]_0 - \left[AB\ 113\right]_t}{\left[AB\ 113\right]_0} \times 100 \qquad (2)$$

$$TOC\ removal\ (\%) = \frac{\left[TOC\right]_0 - \left[TOC\right]_t}{\left[TOC\right]_0} \times 100 \qquad (3)$$

where AB113 removal (%) shows AB113 dye removal efficiency, $[AB113]_0$ and $[AB113]_t$ represents the initial concentration of AB113 at the time 0 and the concentration of AB113 at time t, respectively. $[TOC]_0$ and $[TOC]_t$ is related to the TOC before and after treatment, respectively.

The required air was supplied to the reactor through an air pump (Model SB-118). TOC analyzer (Elementar, Germany) was used to measure the TOC content of the AB113 dye. Intermediate compounds produced during the process were measured by liquid chromatography coupled to mass spectrometry (LC-MS) analysis (Quattro Micro API micro mass Waters 2695) [60]. For this purpose, the mobile phase consisted of acetonitrile containing 0.1% formic acid and water containing 0.1% formic acid with a ratio of 70:30 at a flow rate of 0.25 mL/min. Also, the column used in this device was Atlantis T3-C18 (Dimensions of 3 μ, 2.1 × 100 mm). The detector used was electron spray ionization with the positive scan mode at 40 V.

Structure and characteristics of activated carbon and graphite electrode after reaction were assessed using the analyses, for example, scanning electron microscopy (SEM) (model HITACHI S-4160, Japan) and X-ray diffraction (XRD pattern) by X'Pert Pro diffractometer (Rigaku RINT2200, Japan).

2.3. 3D/EPS catalyzed by GAC process

The present study is an experimental study that was conducted to investigate the applicability of the 3D/EPS system in the removal of AB113 dye. A 400 mL electrochemical reactor made of Plexiglass (with the discontinuous flow) filled with 250 ml water was used as the desired pilot. The dimensions of two electrodes used in the present study were 10 cm × 6 cm × 0.5 cm and the distance between them was 4 cm. The electrodes were placed vertically and parallel to each other and were floated in solution. The schematic of this reactor was represented in Fig. 1.

The graphite electrode was used as the anode, and SS was applied as the cathode; the GAC was poured into the plastic grid and inserted as the third dimension between these two electrodes [50]. GAC was considered as the particle electrode and third dimension of the process due to the characteristics including low cost, chemical stability, and high surface area.

The anode and cathode electrodes were connected to the direct current generator device (PS-405 model) by interface wires. The required mixing in the reaction reactor was provided by a magnetic magnet at a speed of 150 rpm. In this study, at the first stage, the effect of the main variables including pH (in the range of 3–11), GAC dosage (in the range of 2.5–2.5 g), persulfate concentration (in the range of 5–25 mM), electrode potential (in the range of 3–15 V), and the reaction time (5–25 min) on 3D/EPS process performance was investigated at a constant concentration of

Table 1
Characteristics of acid blue 113 dye [12,49]

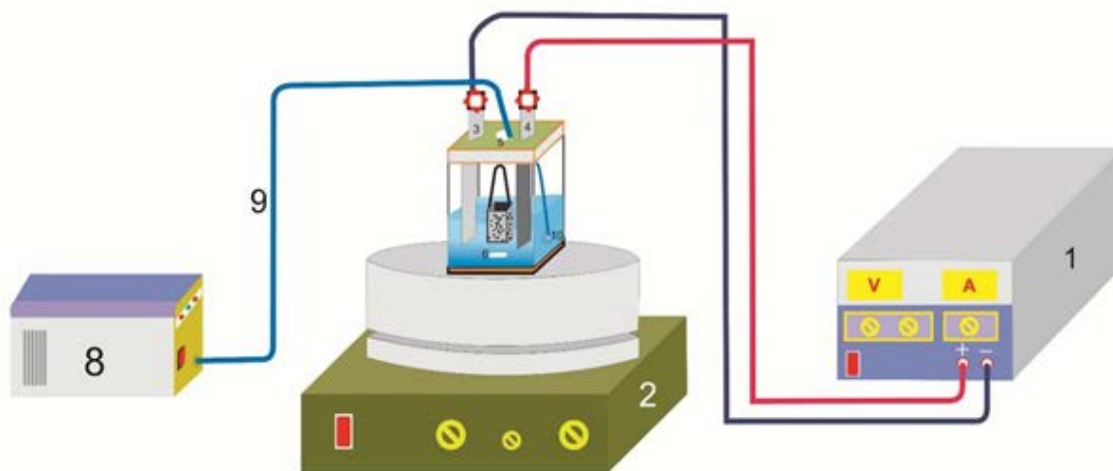| Chemical name	Acid Blue 113
Dye type	Diazo
Chemical structure	
Solubility in water	40 mg/L
Dye index	CI2630
Appearance characteristic	Dark blue powder
Molecular (chemical) formula	$C_{32}H_{21}N_5Na_2O_6S_2$
IUPAC name	Disodium 8-anilino-5-[[4-(3-sulfonatophenyl) azo-1-naphthyl] azo] naphthalene-1-sulfonate
Molar mass	681.65 g/mol
Other name	Acid Fast Blue 5R
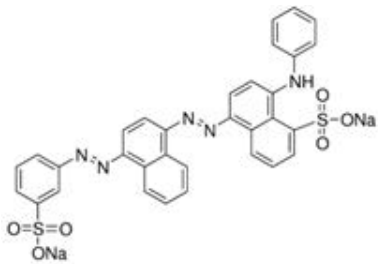
Fig. 1. Schematic of 3-Dimensional electro persulfate. (1) Power supply, (2) magnetic stirrer, (3) cathode electrode (stainless steel), (4) anode electrode (graphite), (5) 3-Dimensional electrochemical reactor, (6) magnet, (7) plastic grid containing the GAC, (8) air pump, (9) air hose, and (10) air rock.

AB113 dye (100 mg/L) and constant aeration rate (75 ml/min) and considering the distance between electrodes of 4 cm [51–58]. The experimental range and levels of independent variables studied for AB113 degradation at five levels are shown in Table 2. The values of the variables and their variation limits were selected based on preliminary experiments. During these experiments, AB113 degradation efficiency was used to evaluate the effectiveness of the process. Table 3 shows the experimental conditions according to the factorial design. The measured responses include the degradation of AB113 dye using the 3D/EPS process. The results obtained based on CCD were analyzed using analysis of variance (ANOVA) variable analysis and multiple regression analysis. Furthermore, the results can be demonstrated by a 3D plot regarding the simultaneous effect of independent variables on the responses. The effectiveness of the fit of the model was represented by the determination coefficient (R^2). Model terms were determined by the p-value and the F-value. The ANOVA and other statistical data were calculated and generated using the Design Expert Software version 11.0.

A direct current (DC) power supply (DAZHENG PS-305D, China) with an electric current of 0–5 A and voltage of 0–30 V was used to supply the electrical current. All batch experiments were performed at room temperature in duplicate.

3. Results and discussion

3.1. Structure and characterization of the properties of granular activated carbon and graphite electrode

Scanning electron microscopy (SEM) technique was used to evaluate the microstructures of the GAC substrate and graphite electrode, and the SEM image of the GAC at different magnifications (3, 5, and 20 μm) has been shown in Fig. 2 and the SEM image of the graphite electrode has been represented in Fig. 3.

Table 2
Levels and ranges of variables studied in the removal of Acid blue 113 dye

Factors	Symbol	Unit	Levels				
			$-\alpha$	-1	0	$+1$	$+\alpha$
pH	A	–	3	5	7	9	11
PS	B	mM	5	10	15	20	25
Voltage	C	V	3	6	9	12	15
GAC	D	Gr	2.5	5	7.5	10	12.5
Time	E	min	5	10	15	20	25

According to the results, the GAC surface, which was highly porous before the reaction [59], can trap and retain the intermediate compounds produced after the reaction on the porous surface.

Furthermore, the results showed that the surface of the graphite electrode was initially smooth and almost uniform. After the reaction, these plates have been broken as shown in Fig. 3 and become irregularly crystalline.

The XRD image obtained from the GAC after the reaction has illustrated in Fig. 4. Crystalline portions of the sediments with transparent peak [silicon oxide (SiO_2) and calcium carbonate ($CaCO_3$) compounds] has well identified on the GAC surface as by-products in the electrolysis reaction [60].

3.2. Process analysis and modeling with central composite design

In this study, the central composite design (CCD) model was used to evaluate the interactive effect of parameters for optimizing the removal of AB113 dye from aqueous solutions using 3D/EPS catalyzed by the GAC process.

Based on the results, the 3D/EPS efficiency catalyzed by the GAC process in the removal of AB113 dye, according to

Table 3
Designed Experiments by software for removal of Acid Blue 113 dye using 3D/EPS Process with GAC Catalyst

Run	pH	PS	Voltage	GAC	Time	Experimental removal	Predicted removal
1	9	10	6	5	10	55.2	55.36
2	7	15	9	7.5	15	74.6	74.25
3	7	15	9	12.5	15	80.7	81.01
4	7	25	9	7.5	15	76.2	76.67
5	9	10	12	5	20	65.6	65.27
6	9	20	6	10	20	75.7	74.92
7	7	15	3	7.5	15	66.2	66.85
8	9	10	12	5	10	61.3	61.11
9	5	10	12	10	20	77.1	77.52
10	5	10	6	10	20	72.1	71.76
11	7	15	9	7.5	15	73.5	74.25
12	9	10	6	10	20	67.5	67.67
13	5	10	12	5	20	69.1	69.36
14	11	15	9	7.5	15	63.2	63.15
15	7	15	9	7.5	5	68.8	68.95
16	3	15	9	7.5	15	71.2	72.06
17	9	10	6	10	10	63.6	63.51
18	5	10	6	5	20	63.9	63.61
19	5	20	12	10	20	86.1	85.49
20	7	15	9	7.5	15	73.8	74.25
21	9	20	6	5	20	66.5	66.77
22	7	15	15	7.5	15	78.2	78.36
23	5	20	12	10	10	81.6	81.34
24	7	5	9	7.5	15	61.1	61.44
25	9	20	12	5	10	68.8	68.37
26	9	20	12	10	10	76.3	76.52
27	5	10	6	5	10	60.3	59.45
28	5	20	12	5	20	77.9	77.34
29	5	20	6	10	20	80.3	79.74
30	7	15	9	7.5	15	74.6	74.25
31	5	10	12	5	10	65.3	65.21
32	7	15	9	2.5	15	64.2	64.7
33	7	15	9	7.5	15	74.5	74.25
34	9	10	12	10	10	69	69.27
35	5	20	6	10	10	75.6	75.58
36	5	20	12	5	10	73.1	73.18
37	5	10	12	10	10	73.6	73.36
38	9	10	6	5	20	59.9	59.51
39	9	20	6	10	10	70.7	70.77
40	5	20	6	5	10	67.1	67.43
41	9	10	12	10	20	73.3	73.42
42	7	15	9	7.5	25	76.6	77.26
43	7	15	9	7.5	15	74.5	74.25
44	5	10	6	10	10	67.7	67.61
45	7	15	9	7.5	15	74.6	74.25
46	7	15	9	7.5	15	74.7	74.25
47	9	20	12	10	20	80.4	80.68
48	9	20	12	5	20	72.6	72.52
49	5	20	6	5	20	71.3	71.58
50	9	20	6	5	10	62.6	62.61
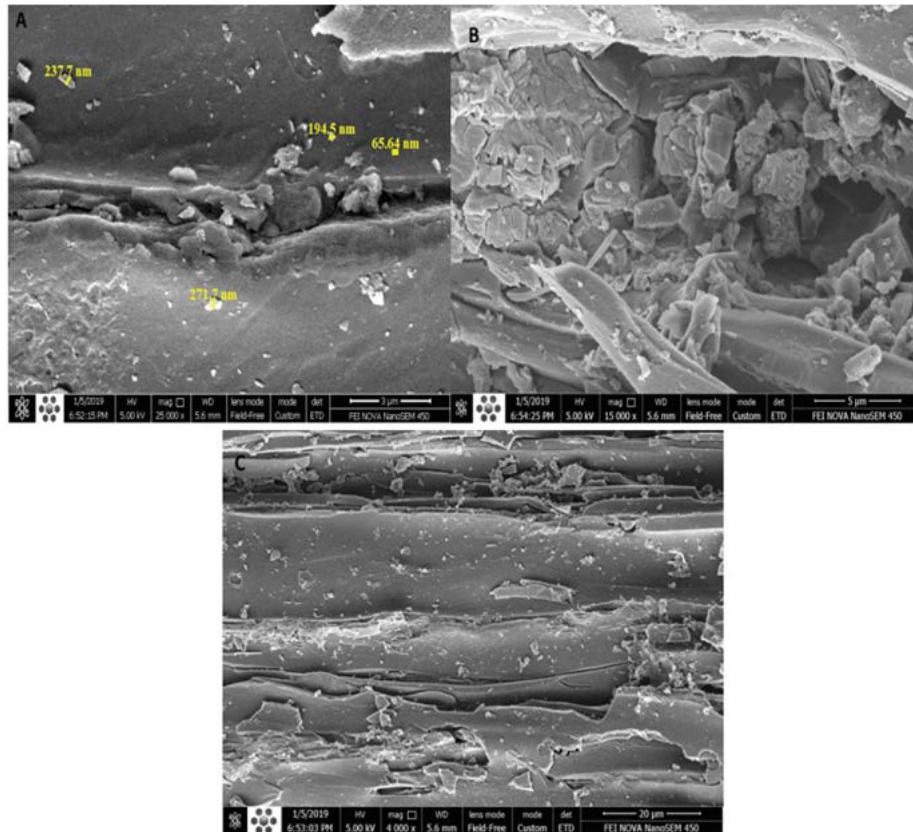
Fig. 2. (a–c) SEM image of the activated carbon surface after reaction (with different magnifications).
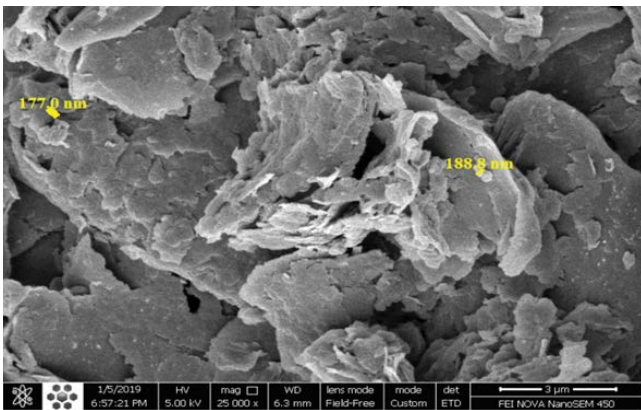
Fig. 3. SEM image of the graphite electrode surface after reaction (magnification × 25,000).

Fig. 4. XRD image of GAC after reaction.

changes in experimental conditions, varies from 55.2% to 86.1% (Table 3).

The first step in analyzing the results is selecting a suitable model for the system that can predict the results accurately. Quadratic models were used for this purpose. ANOVA is often used to evaluate the model and to test its significance. The results related to the removal of AB113 dye by the 3D-EPS process with the GAC catalyst are shown in Table 4. Factors with a *p*-value of <0.05 remained in the model. With regard to the remaining parameters in the system, a model was finally presented to predict the studied dye

removal efficiency. Eq. (5) is the proposed model based on the factors coded in Table 2 which is as follows: In this equation, *X* is the predicted removal efficiency in terms of percentage.

$$X = 74.25 - 4.45A + 7.62B + 5.75C + 8.16D + 4.15E - 0.71AB + 0.44BD - 0.16CE - 6.64A^2 - 5.19B^2 - 1.64C^2 - 1.39D^2 - 1.14E^2 \tag{5}$$

The presented model consists of five variables related to single-component or linear effects (*A*, *B*, *C*, *D*, *E*), five variables related to curve or quadratic effects (A^2, B^2, C^2, D^2, E^2), and three variables related to dual or interaction effects (*AB*,

Table 4
Statistical models obtained from the ANOVA for response surface reduced quadratic model for optimization of Acid Blue 113 dye removal

Source	Sum of squares	df	Mean square	F-value	p-value	
Model	2,102.3	13	161.75	797.02	<0.0001	Significant
A-pH	198.47	1	198.47	977.96	<0.0001	
B-PS	579.88	1	579.88	2,857.36	<0.0001	
C-voltage	331.20	1	331.20	1,631.99	<0.0001	
D-GAC	665.04	1	665.04	3,276.98	<0.0001	
E-time	172.64	1	172.64	850.68	<0.0001	
AB	1.02	1	1.02	5	0.0316	
BD	0.38	1	0.38	1.89	0.1781	
CE	0.053	1	0.053	0.26	0.6131	
A^2	88.25	1	88.25	434.83	<0.0001	
B^2	53.92	1	53.92	265.71	<0.0001	
C^2	5.40	1	5.40	26.59	<0.0001	
D^2	3.88	1	3.88	19.11	<0.0001	
E^2	2.61	1	2.61	12.86	0.001	
Residual	7.31	36	0.20			
Lack of fit	5.93	29	0.20	1.04	0.5237	Not significant
Pure error	1.38	7	0.20			
Cor. total	2,110.04	49				

Model: Quadratic, R^2: 0.9963, $R^2_{Adjusted}$: 0.9953, $R^2_{predicted}$: 0.9915, Adeq. precision: 136.2833, and CV: 0.6353

CE, *BD*). According to the coefficients of the factors in the above equation, the importance of each parameter was clarified, so that the concentration of GAC had the highest importance in the removal of AB113 dye. In addition, the effect of pH on removal was negative, and the removal efficiency at acidic pH was higher. Furthermore, the effect of persulfate concentration, electrode potential, and retention time on removal was observed to be positive. In Eq. (1), *A*, *B*, *C*, *D*, and *E* show pH, persulfate (mM), voltage (V), and reaction time (min), respectively.

The quality of the proposed model is evaluated using the coefficient of determination (R^2). The coefficient of determination is the ratio of the sum of squares described to the sum of total squares, and its numerical value varies between 0 and 1; the selected model has more validity when the R^2 is closer to 1. When $R^2 > 0.9$, the proposed model can be reliably applied to optimize the response. As shown in Table 4, $R^2 = 0.99$, which indicates that the model has acceptable accuracy.

The low values of CV are indicative of excellent accuracy and high reliability of experiments; in this study, this value was observed to be 0.6353. The lack of fit (LOF) is a good predictor of the model. Based on obtained results, LOF for AB113 dye was not significant ($P = 0.0.5237$). Since insignificant LOF is a prerequisite for a flourishing predictive model, like large *p*-values, along with significant regressions ($p < 0.0001$ for the model), it confirms that the model satisfactorily predicts the experimental results at the confidence level of 95%.

Residuals plots are employed to explain the difference between the observed values for a response and its predicted value, which are critical for estimation of the adequacy of the model. In addition, signifying the residuals departure from a straight line is accomplished by Normal test plots which are graphical tools. The normal probability plot of AB113 dye removal using 3D/EPS catalyzed by the GAC process (Fig. 5a) is representative of normal scattering of almost all data points near to the straight line and lack of gross distribution around the line. The adequacy of the model was also assessed by drawing the residuals plot vs. the predicted responses. In Fig 5b, the random scatter of the residuals around the zero is observed, which symbolizes the appropriate behavior of the models and the desirability of constant variance assumptions. In addition, it should be noted that there is no dependency between residuals and time or any other parameters in a well-designed model. In the represented externally studentized residuals vs. the run (Fig. 5c), the independence of the residuals to the runs could be observed for any observable trend. Generally, it was found that the removal of AB113 dye by 3D/EPS catalyzed by the GAC process could be adequately predicted through the proposed model.

The effect of each of the studied factors (pH, persulfate, Voltage, GAS, and reaction time) on the removal of AB113 has shown in Fig. 5d. According to Fig. 5d, all the parameters except for the pH parameter was increased by increasing concentration.
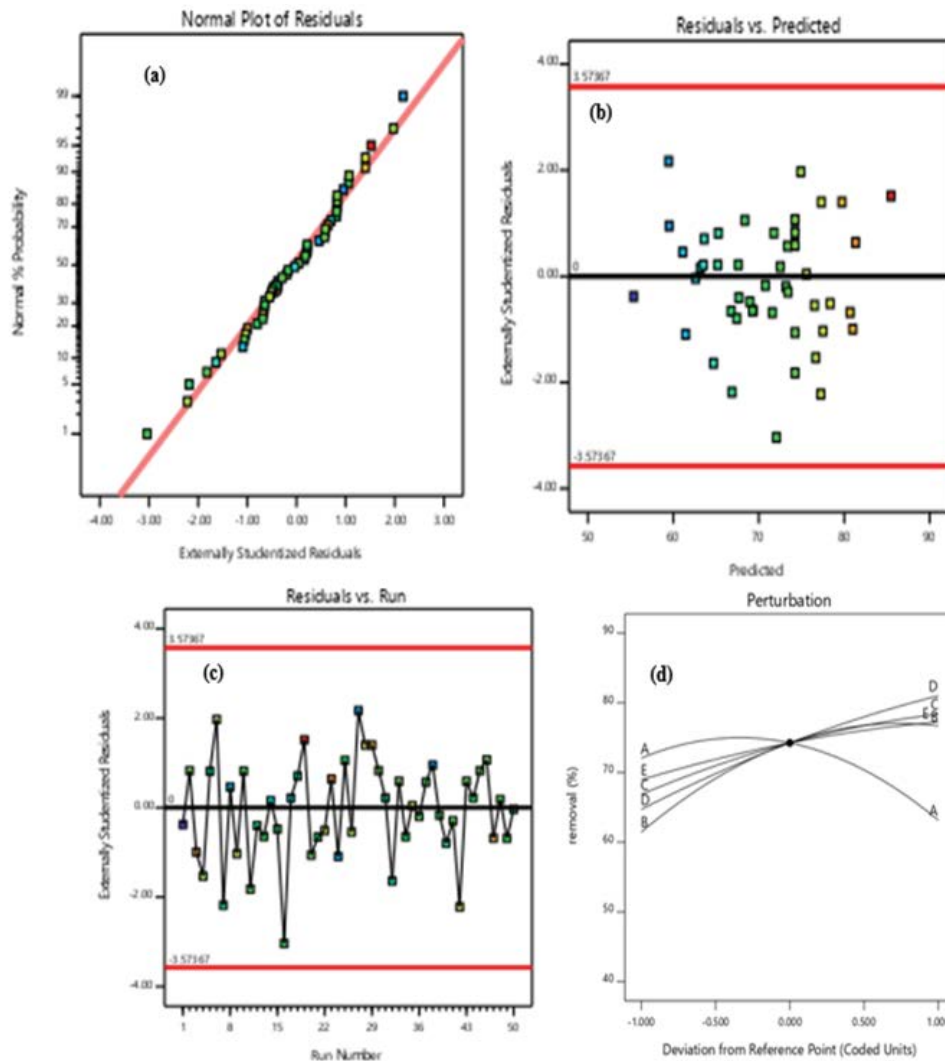
Fig. 5. (a) Normal probability distribution of residuals, (b) residuals vs. predicted, (c) externally studentized residuals vs. run, and (d) Perturbation plot for removal of AB 113 dye.

3.3. Optimization of AB113 dye removal by RSM

Graphical optimization is a multi-layered map to indicate the region in which the response values are obtained. Fig. 6 shows the graphical optimizations, which represent the region that provides the desired response values (yellow region). The optimum region is identified for removal of AB113 dye by 3D/EPS catalyzed by the GAC process, which were considered as criteria. The yellowish zone covers the pH of 7, persulfate of 15 mM, a voltage of 9 V, GAC of 7.5 gr, and reaction time of 15 min. In order to verify the accuracy of the models, one point is selected in optimum areas (conditions shown by the flag are shown in Fig. 6. The 3D/EPS catalyzed by the GAC process was used to compare the actual values with predicted values of responses. Table 5 shows the results of the experiments in optimum areas. The correctness of the optimum conditions with DOE software was examined by the standard deviation for each response. The actual values are very close to the predicted values of the model.

3.4. Interaction effect between initial pH and persulfate concentration in the removal of AB113

Fig. 7 shows the AB113 dye removal efficiency as a function of pH and persulfate concentration. Based on the results of the ANOVA shown in Table 4, $P < 0.05$, and there was a significant relationship between the initial pH and the persulfate concentration in the process studied. It is observed that by increasing persulfate concentration to 22.59 mM, the efficiency was increased and it had a decreasing trend at further concentrations. Moreover, the removal efficiency was increased by increasing the pH from 3 to 5.50, but the reduction in efficiency was observed for the pH values beyond the mentioned values. The highest removal efficiency (91.86%) was observed at pH of 5.5 and persulfate concentration of 22.59 mM, and the lowest removal efficiency was at pH of 11 and persulfate concentration of 5 mM, which was equal to 65.41%. Persulfate not only can produce the sulfate radicals in the degradation of pollutants but also is capable to generate the hydroxyl radicals in direct reaction with water.
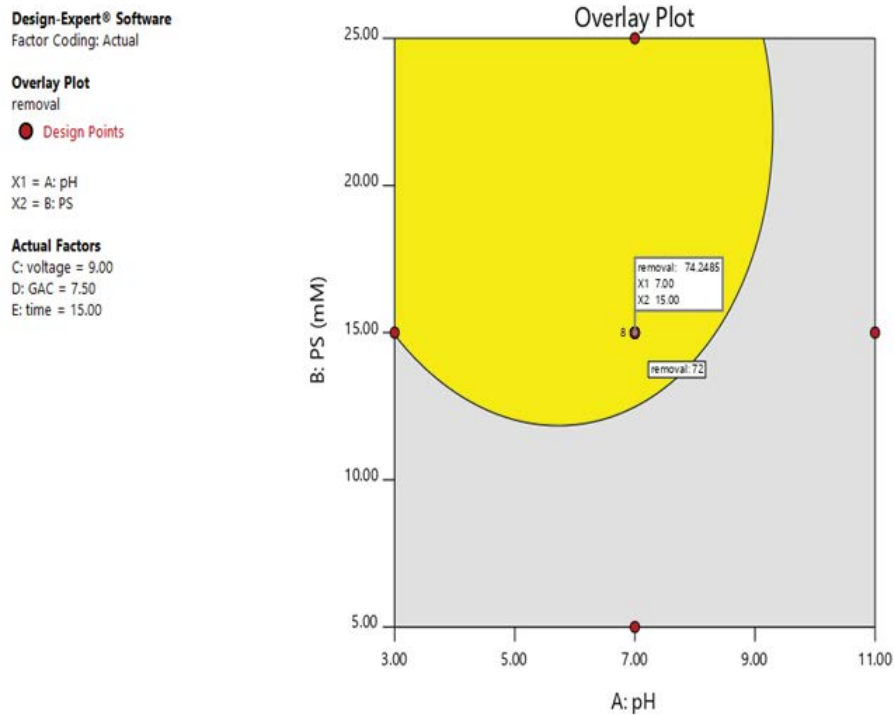
Fig. 6. Overlay plots for the optimal region.

Table 5
Verification of experimental results at optimum conditions

Optimum condition	Acid Blue 113 dye removal (%)
Experimental results	74.25%
Model response	CI low: 73.91, CI high: 74.57
Error	0.163
Standard deviation	±0.47

Therefore, increasing the persulfate, up to a certain concentration, is led to the high production of free radicals and, thus, higher AB116 dye removal efficiency [61].

Moreover, when the persulfate salt in the EPS process is poured in water, the $S_2O_8^{2-}$ anion is formed in water (reaction 6); the $S_2O_8^{2-}$ anion has low oxidation ability and the oxidation of the organic compounds by this anion is slowly performed at ambient temperature and for this reason, the activation of persulfate for the production of $SO_4^{\bullet-}$ radical is required (reaction 7) [61].

$$S_2O_8^{2-} + 2e^- \rightarrow 2SO_4^{2-}, \; E^0 = 2.01 \text{ V} \tag{6}$$

$$SO_4^{\bullet-} + e^- \rightarrow SO_4^{2-}, \; E^0 = 2.6 \text{ V} \tag{7}$$

3.5. Interaction effects between potential electrode and retention time in the removal of AB113

In Fig. 8, the interaction effect between electrode potential and retention time on the AB113 removal is shown as a function of electrode potential and retention time. According to the results of the ANOVA shown in Table 4, $P < 0.05$, and there was no significant relationship between the potential electrode and retention time in the process studied. As can be seen in this Figure, by increasing the electrode potential and the retention time, the AB113 dye removal efficiency was increased. The removal efficiency increases when both parameters are at their highest level so that the lowest removal efficiency was observed at the electrode potential of 3 and the retention time of 5 min, which showed removal efficiency of 72.11%. Our results are agreed with the results obtained by Dargahi et al. [62] and Samarghandi et al. [63].

The results of the study conducted by Dargahi et al. [62] and Samarghandi et al. [63] showed that increasing the voltage is led to increasing the pollutant degradation efficiency [62].

The results also showed that reaction time has a direct relationship with the removal efficiency of AB113, so that by increasing electrolysis time, the dye removal efficiency was also increased because an increase in the electrolysis time leads to enhancing the production of the hydroxyl radicals and, as a result, increasing the dye removal efficiency by the 3D/EPS process [63].

3.6. Interaction effects between persulfate concentration and GAC mass in the removal of AB113 dye

In Fig. 9, the interaction effect of persulfate concentration and GAC mass in the removal of AB113, as a function of persulfate concentration and GAC mass, has shown. Considering the results of the ANOVA reported in Table 4, $P < 0.05$, and there was no considerable relationship between the concentration of persulfate and the GAC mass in the
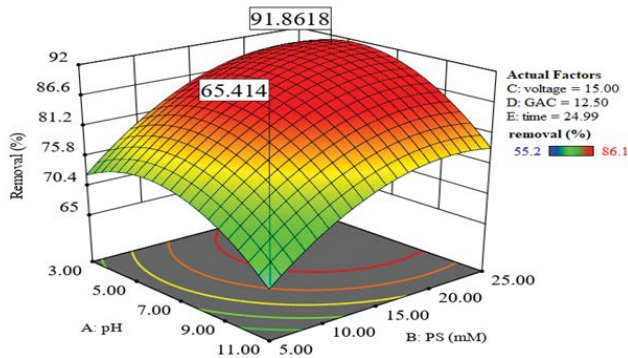
Fig. 7. Acid Blue 113 dye removal efficiency as a function of initial pH and PS concentration at electrode potential of 15 V and GAC concentration of 12.50 g and retention time of 25 min.
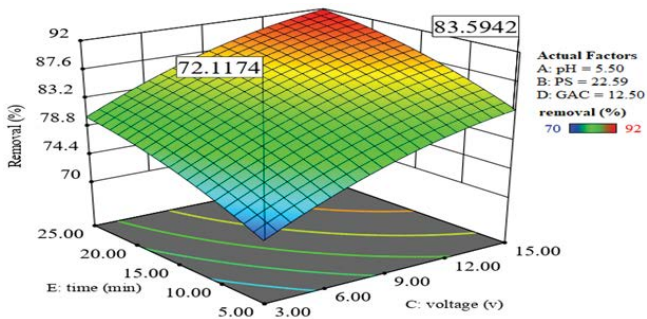
Fig. 8. Acid Blue 113 dye removal efficiency as a function of electrode potential and retention time at pH of 5.50, PS concentration of 22.59, and GAC of 12.50 g.
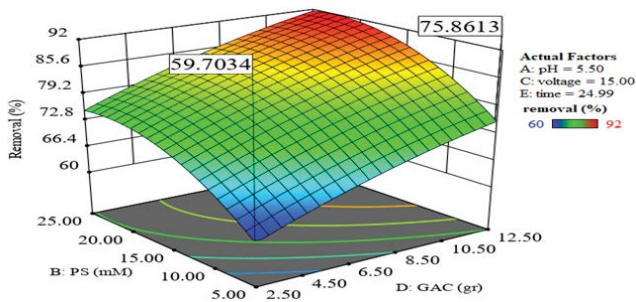

Fig. 9. Acid Blue 113 dye removal efficiency as a function of pre-sulfate concentration and GAC mass at pH of 5.50 and electrode potential of 15 V and retention time of 24.99 min.

process studied. As can be seen in Fig. 9; increasing the GAC mass has led to enhance the AB113 dye removal efficiency, and the highest removal efficiency was for the persulfate concentration of 22.59 mM; so that the lowest removal efficiency (59.70%) was observed at the persulfate concentration of 5 and GAC mass of 5 g.

3.7. Effect of the distance between electrodes on AB113 dye removal

After optimizing initial solution pH, persulfate concentration, electrode potential and retention time and GAC dosage,
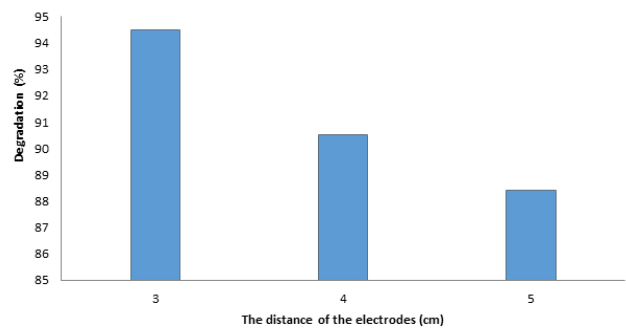
Fig. 10. The effect of distance between electrodes on the removal of acid blue 113 dye under optimum conditions.

the effect of distance between electrodes were investigated under optimum conditions. Fig. 10 shows the results of this section. As observed, the removal efficiency was decreased by increasing the distance. In other words, the distance between the electrodes is inversely correlated with the dye removal efficiency. So that when the distance between the electrodes is increased, the electrical resistance between the electrodes is also increased, and according to Ohm's law, if the voltage is constant, the electric current decreases. Accordingly, this decrease in current is led to producing fewer gas bubbles and their deformation in size. Therefore, the removal efficiency is reduced. When the distance between the electrodes decreases, the gas bubbles create effective hydrodynamic turbulence so that the efficiency is effectively enhanced [64]. According to studies by Merzouk et al. [65] for the treatment of textile industry wastewater through electrocoagulation, it was detected that the pollutant removal efficiency was decreased by increasing the distance between the electrodes from 1 to 3 cm.

3.8. Effect of aeration and nitrogenation on AB113 dye removal

In order to investigate the effect of aeration and nitrogenation on the AB113 dye removal in the 3D/EPS process, samples were prepared under optimum conditions and air and nitrogen were sprayed with flow rates of 0, 75, and 150 ml/min. The results were represented in Figs. 11a and b. As can be seen, spraying air and nitrogen into the studied samples reduces and increases the process efficiency, respectively. The reason can be explained that in AOPs based on the use of persulfate in the electrochemical environment, the diffusion of nitrogen gas (N_2) and oxygen gas (O_2) can affect the formation and consumption of radicals due to secondary reactions at the cathode and anode electrodes surface. In order to develop the efficiency of the sulfate radical in aqueous environments, nitrogen gas enters the environment and this phenomenon can be described by this fact that, by the introduction of N_2 gas, the O_2 produced by anodic oxidation of the water is existed from the environment and is led to absorb a large number of persulfate anions on the cathode. Therefore, more sulfate radicals are produced. In other words, an increase in the number of sulfate radicals produced is attributed to the cathodic reduction of the persulfate anions, which can compete with O_2 to absorb electrons (reactions 8 and 9).
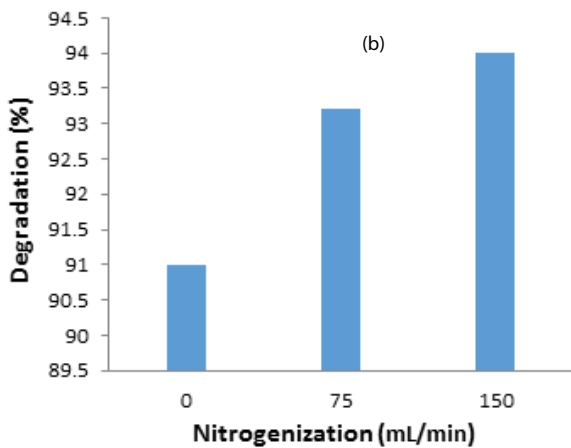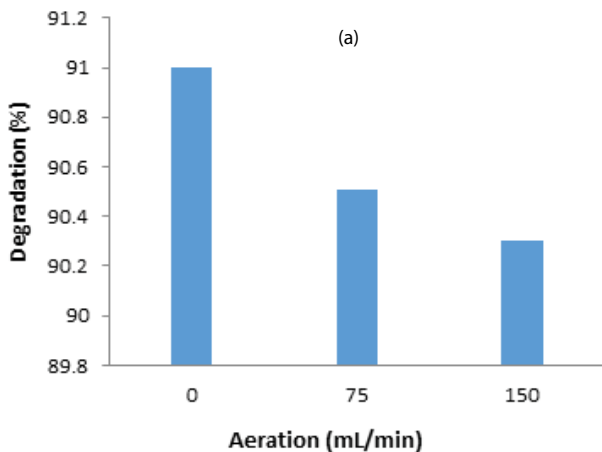
Fig. 11. (a) Effect of aeration on the acid blue 113 dye removal under optimum conditions and (b) Effect of nitrogenation on the acid blue 113 dye removal under optimum conditions.

$$S_2O_8^{2-} + e^- \rightarrow SO_4^{\bullet-} + SO_4^{2-} \qquad (8)$$

$$O_2 + 2H^+ + 2e \rightarrow H_2O_2 \qquad (9)$$

Thus, the main mechanism is to promote the formation of $SO_4^{\bullet-}$ through cathodic reduction of anion sulfate [43]. Chen et al. [66] have obtained similar results in their study, which was conducted to eliminate the toxic compound of dinitrotoluene. Conversely, an increase in O_2 concentration has resulted in the reduction of the formation of $SO_4^{\bullet-}$ due to the creation of the competition with persulfate anion in the capture of the electron [66].

3.9. Effect of the initial concentration of AB113 dye on AB113 dye removal

In order to investigate the effect of the initial concentration of AB113 dye, three different initial concentrations of AB113 were tested under optimum conditions. In the similar experimental parameters, the number of activated radical species resulted from this process was assumed to be constant.
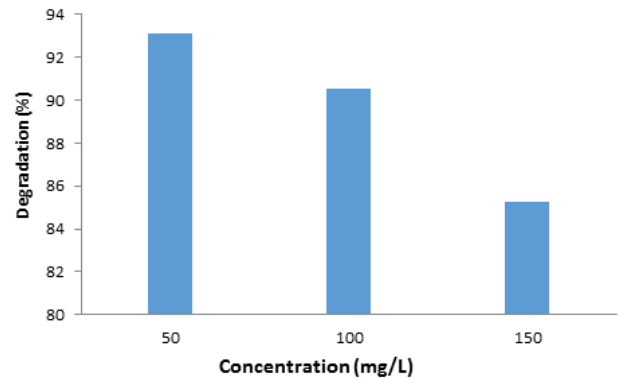
Fig. 12. Influence of initial dye concentration on the acid blue 113 dye removal under optimum conditions.
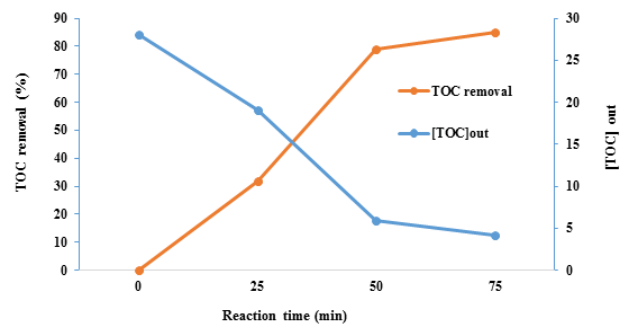
Fig. 13. Decreasing trend of TOC in optimal conditions.

As shown in Fig. 12, the removal efficiency was decreased from 93.11% to 93.85% by an increase in the concentration of AB113 from 50 to 100 mg/L. By increasing the dye concentration to 150 mg/L, the efficiency was decreased to 58.25%. In other words, the removal efficiency of the dye has reduced by increasing the initial concentration of AB113, which can be attributed to the decrease in oxidized molecules. In addition, the increase in dye concentration leads to decreasing the concentration of the produced radicals and to decline the chance of collision between the produced radicals and the dye molecules; this obviously results in reducing the dye removal efficiency [67].

3.10. Mineralization of AB113

To estimate the effective role of the 3D/EPS process in degradation and mineralization of AB113, the TOC removal efficiency in optimal condition was determined (Fig. 13). The results showed that increasing the reaction time is led to improving the dye degradation rate; so that by an increase in the reaction time from 0 to 75 min, the TOC removal rate was increased to 85% by 3D/EPS process. Accordingly, the TOC was decreased from 28 to 4.2 mg/L by increasing the reaction time from 0 to 75 min (Fig. 13).

3.11. Influence of each factor on the AB113 dye removal process

Fig. 14 reveals the percentage effect of each significant factor on the removal of AB113. As can be seen, and according
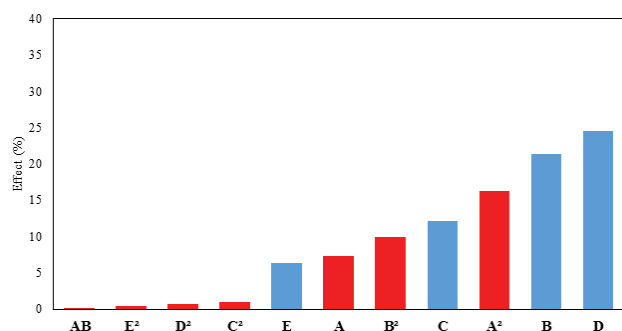
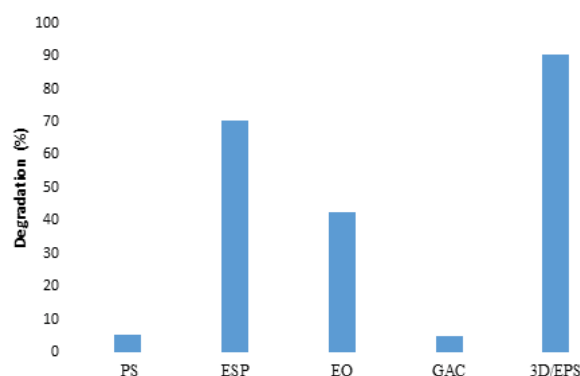Fig. 14. Effect of each term on AB113 removal (■ Positive effect, ■ Negative effect).

Fig. 15. Effect of separate and 3D/EPS processes on the removal of acid blue dye 113 under optimum conditions.

to the variables coded in Table 2, the percentage of the positive effect of GAC dosage and persulfate concentration was higher than other factors. In general, the effect of independent variables on the removal efficiency of AB113 dye has been illustrated by blue and red colors to show positive and negative effects, respectively [68].

3.12. Determination of the synergistic effect of different components of the 3D/EPS process on the removal of AB113 dye

To investigate the effect of AB113 dye on 3D/EP process systems, five separate samples containing 100 mg/L dye solution were prepared. It should be noted that all processes were performed in optimal conditions. In the first sample, only peroxodisulfate (PDS) was used to remove the dye. It was observed that the dye removal was low (5.4%) due to the stability of PDS at ambient temperature and its limited oxidation capacity [53]. Consequently, other samples were investigated to evaluate the effect of electropersulfate process and the effect of the electrochemical process without the presence of persulfate and the effect of the process in the presence of GAC alone and the effect of the EPS process in the presence of GAC. The retention time in all samples was 25 min. The results obtained were presented in Fig. 15. Separate electropersulfate process, at the end of the process, removed about 70.25% of the dye; under the same conditions, the electrochemical process without the presence of persulfate was capable to provide only 42.6% removal efficiency, while the EPS process in the presence of GAC was able to remove 91.85% of the studied dye. The net effect of GAC was evaluated as the third dimension. The process in the presence of GAC only removed 5% of the dye.

In other words, the efficiency of the two-dimensional (2D) process was 70.25% at optimum conditions, which were significantly lower than the efficiency obtained by its three-dimensional (3D) process. Since, prior to the start of the electrochemical process, the GAC particles have been immersed in the AB113 dye solution, and no significant adsorption could be observed; thus, this increase in efficiency could be attributed to the electrochemical role of GAC. GAC, due to having poly aromatic components (PACs) and functional groups, can significantly improve the desired radicals in the removal of the dye through the 3D-EPS process compared to the 2D process type [46]. On the other hand, each GAC particle plays a microelectrode in the induced electric field due to its high electrical conductivity, which improves the direct oxidation of the target pollutant by reducing the distance of pollutant movement to the electrode surface [69].

3.13. Intermediate products produced by 3D/EPS process for removal of AB113 dye under optimum conditions and its proposed degradation pathways

The degradation of AB113 dye during the 3D/EPS process in optimum conditions was also confirmed by the chromatogram of LC-MS, as shown in Fig. 16. Based on the LC-MS chromatogram diagram, the M/Z value, chemical name, molecular formula, and structural formula of intermediate materials identified are given in Table 6. Then, the acceptable degradation pathway according to the produced intermediate products was proposed according to the LC-MS diagram, shown in Fig. 17.

The production of powerful radicals, that is, $SO_4^{\bullet-}$ and $^{\bullet}OH$, is fundamentally important and plays an irreplaceable role in the persulfate oxidative system. Therefore, both $SO_4^{\bullet}$ and $^{\bullet}OH$ are perhaps responsible for the degradation of AB113 in aqueous solutions by the electrochemical oxidation system. $SO_4^{\bullet}$ and $^{\bullet}OH$ are electrophilic which preferably remove electrons from an organic molecule. Thus, based on our major reactive species, a tentative pathway for the degradation of AB113 using the studied system was proposed.

Through the analysis of LC-MS, six intermediates were identified; these intermediates was including naphthalen-1-ol, phthalic acid, malonic acid, Malic acid, naphthalene-1,4-diamine, (naphthalen-1-ylsulfonyl)-l¹-oxidane. With the help of $SO_4^{\bullet}$ and $^{\bullet}OH$ radicals, AB113 was cleaved to form, (*A*1, *A*2, *A*3, *A*4, *A*7, *A*8, *A*9) or (*A*5, *A*6). For compound (*A*5, *A*6, *A*9), these could be oxidized by $SO_4^{\bullet}$ and $^{\bullet}OH$ radicals to form naphthalene-1,4-diamine and (naphthalen-1-ylsulfonyl)-l1-oxidane and then these were oxidized to form naphthalen-1-ol, phthalic acid under the oxidation of $SO_4^{\bullet}$ and $^{\bullet}OH$ radicals. However, naphthalen-1-ol, phthalic acid can be degraded in the electrochemical oxidation system. When the electrochemical oxidation system degraded AB113, H_2O, and CO_2 are produced as the final product.
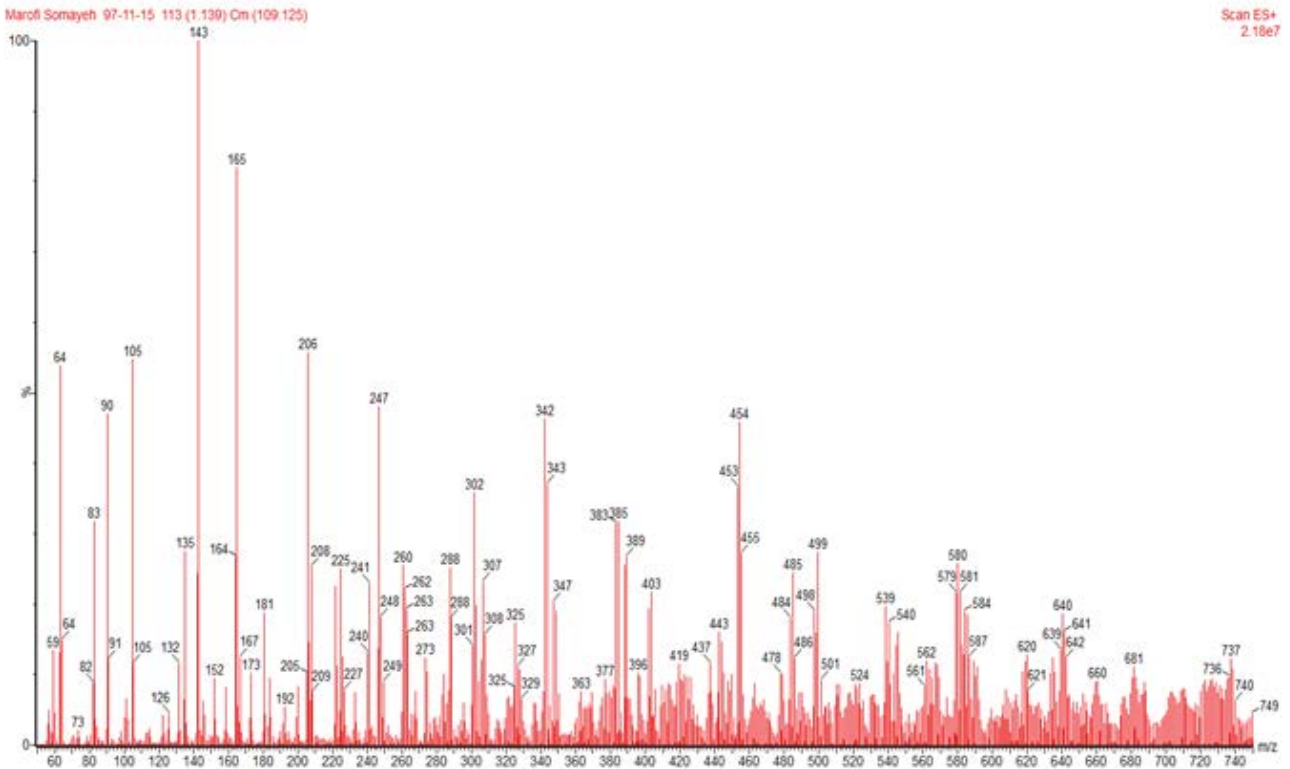
Fig. 16. LC-MS chromatogram after degradation of acid blue 113 dye under optimum conditions.

Table 6
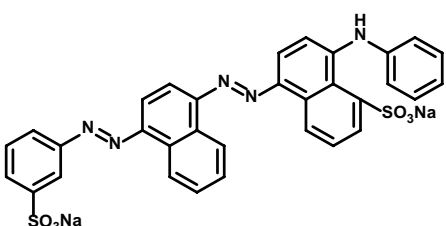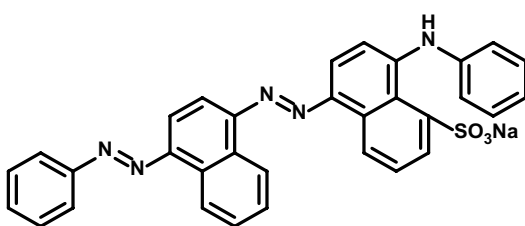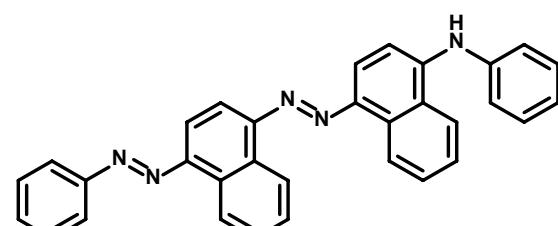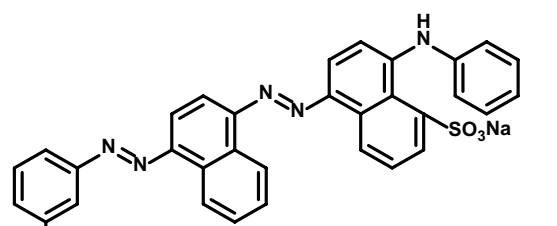Intermediate products produced during the 3D/EPS process

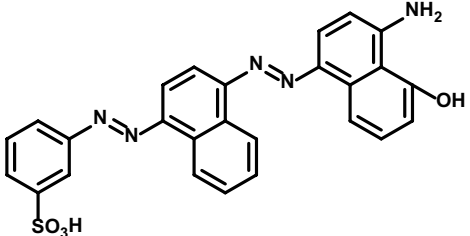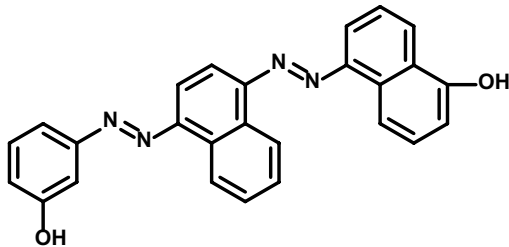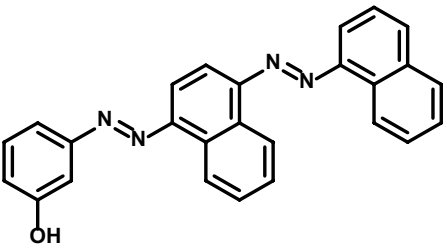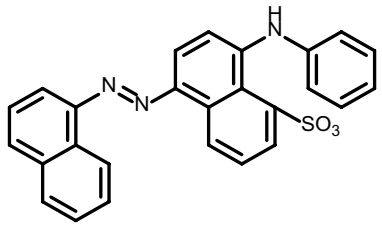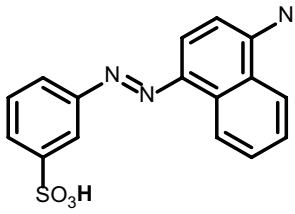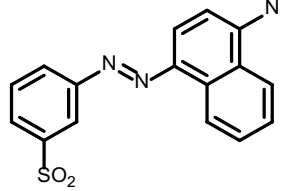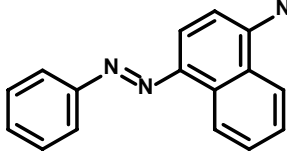| m/z	Structural formula, chemical name, and molecular formula	m/z	Structural formula, chemical name, and molecular formula
681	sodium 8-(phenylamino)-5-((4-((3-sulfonatophenyl)diazenyl)naphthalen-1-yl)diazenyl)naphthalene-1-sulfonate Chemical Formula: $C_{32}H_{21}N_5Na_2O_6S_2$	580	sodium 8-(phenylamino)-5-((4-(phenyldiazenyl)naphthalen-1-yl)diazenyl)naphthalene-1-sulfonate Chemical Formula: $C_{32}H_{22}N_5NaO_3S$
478	N-phenyl-4-((4-(phenyldiazenyl)naphthalen-1-yl)diazenyl)naphthalen-1-amine Chemical Formula: $C_{32}H_{23}N_5$	660	sodium 8-(phenylamino)-5-((4-((3-sulfophenyl)diazenyl)naphthalen-1-yl)diazenyl)naphthalene-1-sulfonate Chemical Formula: $C_{32}H_{22}N_5NaO_6S_2$

Table 6
(*Continued*)

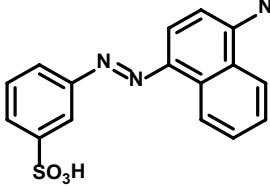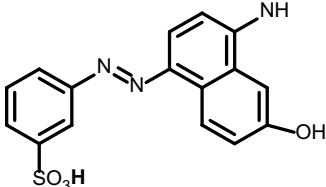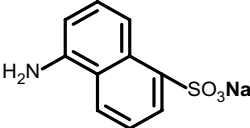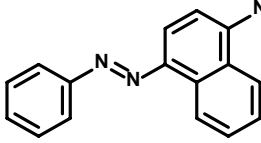| m/z	Structural formula, chemical name, and molecular formula	m/z	Structural formula, chemical name, and molecular formula
499	3-((4-((4-amino-5-hydroxynaphthalen-1-yl)diazenyl)naphthalen-1-yl)diazenyl)benzenesulfonic acid Chemical Formula: $C_{26}H_{19}N_5O_4S$	419	5-((4-((3-hydroxyphenyl)diazenyl)naphthalen-1-yl)diazenyl)naphthalen-1-ol Chemical Formula: $C_{26}H_{18}N_4O_2$
403	3-((4-(naphthalen-1-yldiazenyl)naphthalen-1-yl)diazenyl)phenol Chemical Formula: $C_{26}H_{18}N_4O$	389	4-((4-aminonaphthalen-1-yl)diazenyl)-*N*-phenylnaphthalen-1-amine Chemical Formula: $C_{26}H_{20}N_4$
454	8-((l^1-oxidaneyl)dioxo-l^6-sulfaneyl)-4-(naphthalen-1-yldiazenyl)-*N*-phenylnaphthalen-1-amine Chemical Formula: $C_{26}H_{18}N_3O_3S$	325	3-((4-(λ^1-azaneyl)naphthalen-1-yl)diazenyl)benzenesulfonic acid Chemical Formula: $C_{16}H_{11}N_3O_3S$
308	(3-((4-(l^1-azaneyl)naphthalen-1-yl)diazenyl)phenyl)-l^5-sulfanedione Chemical Formula: $C_{16}H_{10}N_3O_2S$	247	1-(4-(l^1-azaneyl)naphthalen-1-yl)-2-phenyldiazene Chemical Formula: $C_{16}H_{11}N_3$
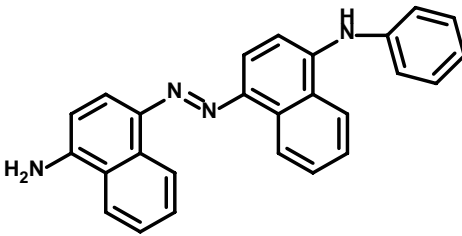
Table 6
(*Continued*)

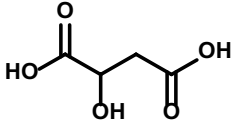| m/z	Structural formula, chemical name, and molecular formula	m/z	Structural formula, chemical name, and molecular formula
325	**3-((4-(λ^1-azaneyl)naphthalen-1-yl)diazenyl)benzenesulfonic acid** Chemical Formula: $C_{16}H_{11}N_3O_3S$	342	**3-((4-(λ^2-azaneyl)-6-hydroxynaphthalen-1-yl)diazenyl)benzenesulfonic acid** Chemical Formula: $C_{16}H_{12}N_3O_4S$
247	**sodium 5-aminonaphthalene-1-sulfonate** Chemical Formula: $C_{10}H_8NNaO_3S$ And **1-(4-(λ^1-azaneyl)naphthalen-1-yl)-2-phenyldiazene** Chemical Formula: $C_{16}H_{11}N_3$	159	**naphthalene-1,4-diamine** Chemical Formula: $C_{10}H_{10}N_2$
173	**8-amino-5-(l^1-azaneyl)naphthalen-1-ol** Chemical Formula: $C_{10}H_8N_2O$	222	**(5-((l^1-oxidaneyl)dioxo-l^6-sulfaneyl)naphthalen-1-yl)-l^2-azane** Chemical Formula: $C_{10}H_7NO_3S$
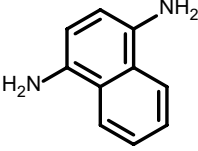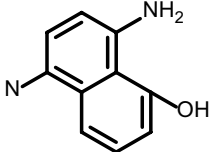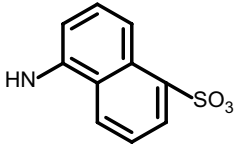
Table 6
(*Continued*)

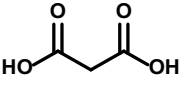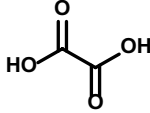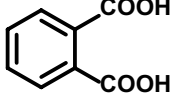| m/z	Structural formula, chemical name, and molecular formula	m/z	Structural formula, chemical name, and molecular formula
143	**naphthalen-1-yl-λ^2-azane** **Chemical Formula: $C_{10}H_8N$** and **naphthalen-1-ol** **Chemical Formula: $C_{10}H_8O$**	206	**(naphthalen-1-ylsulfonyl)-l^1-oxidane** **Chemical Formula: $C_{10}H_7O_3S$**
383	**sodium 5-(naphthalen-1-yldiazenyl)naphthalene-1-sulfonate** **Chemical Formula: $C_{20}H_{13}N_2NaO_3S$**	135	**2-hydroxysuccinic acid** **Chemical Formula: $C_4H_6O_5$**
105	**malonic acid** **Chemical Formula: $C_3H_4O_4$** and **NaHSO3** **sodium hydrosulfonyl-l^1-oxidane**	90	**oxalic acid** **Chemical Formula: $C_2H_2O_4$**
64	**SO$_2$** **sulfur dioxide**	165	**phthalic acid** **Chemical Formula: $C_8H_6O_4$**
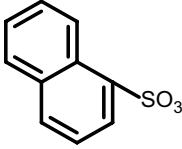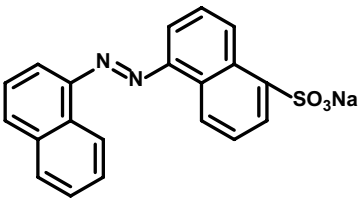
3.14. Comparison of EPS process with other studies

In Table 7, various studies on the removal of various pollutants by the 2D-EPS process. With regard to Table 7, it can be seen that the results of the present study are of some importance compared to the studies mentioned. For example, compared to other studies, in this study, the reduction of AB113 at medium pH (pH 5.5), reaction time (25 min), persulfate (22.59 mmol), and voltage (15 V) was done. Also, considering the lower reaction time of the present study than other studies, dye removal efficiency in the present study is much higher than other similar studies.
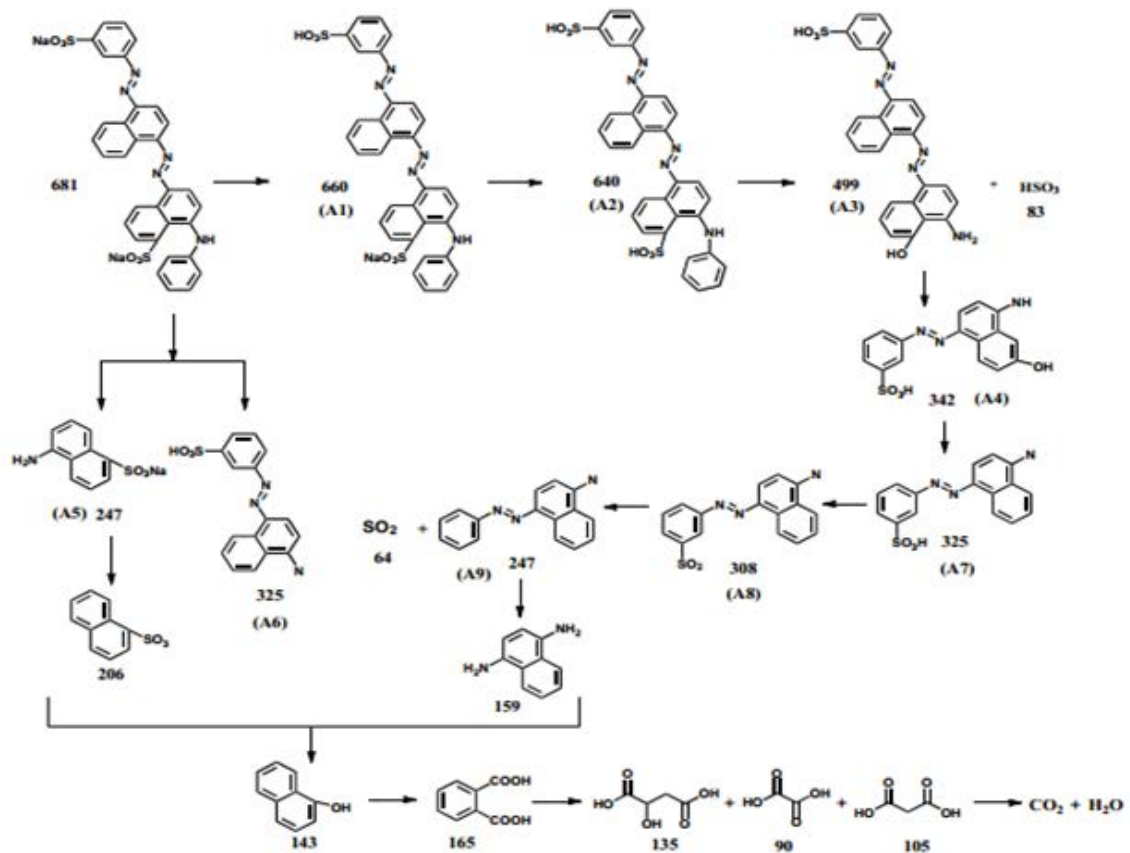
Fig. 17. Proposed acid Blue 113 degradation pathway during 3D/EPS process under optimum conditions.

Table 7
Results of degradation of organic pollutants in aqueous solutions by two-dimensional electro persulfate systems

Pollutant	Concentration	Conditions for testing	Results	Ref.
Aniline	60 mg/L	pH = 3 Voltage = 6V PS = 3% weight Time = 420 min	ND	[67]
Tetracycline	50 mg/L	pH = 4.42 Voltage = 6V PS = 50 mg/L Time = 240 min	81.1%	[33]
Sodium dodecyl ben-zene sulfonate) (SDS	100 mg/L	pH = 3 PS = 25 Mmol Voltage = 10 V Time = 25 min	80%	[70]
Dinitrotoluene	300 mg/L	pH = 5 PS = 1.7 weight Voltage = 6V Time = 480 min	ND	[43]
Acid Blue 113	100 mg/L	pH = 5.5 PS = 22.59 Mmol Voltage = 15 V Time = 24.99 min	70.25%	Current study

4. Conclusion

The results indicate the effective performance of the RSM in optimizing the three-dimensional electro persulfate (3D-EPS) process in the removal of the AB113. Among the studied parameters, the most effective parameter was the GAC dosage and the optimum amount of GAC was considered to be 12.5 g. There is a direct relationship between the dye removal efficiency and persulfate concentration, electrode potential and retention time. Under optimum conditions, this process has an efficiency of 90.51% which is higher than its separate processes.

Acknowledgment

References

[1] A. Dargahi, M. Mohammadi, F. Amirian, A. Karami, A. Almasi, Phenol removal from oil refinery wastewater using anaerobic stabilization pond modeling and process optimization using response surface methodology (RSM), Desal. Water Treat., 87 (2017) 199–208.

[2] A. Seid-Mohammadi, Z. Ghorbanian, G. Asgarai, A. Dargahi, Degradation of CEX antibiotic from aqueous environment by US/S2O82–/Nio process: optimization using taguchi method and kinetic studies, Desal. Water Treat., 171 (2019) 444–455.

[3] A. Seid-Mohammadi, G. Asgari, A. Dargahi, M. Leili, Y. Vaziri, B. Hayati, A.A. Shekarchi, A. Mobarakian, A. Bagheri, S.B. Nazari Khanghah, A. Keshavarzpour, A comparative study for the removal of Methylene blue dye from aqueous solution by novel activated carbon based adsorbents, Prog. Color Colorants Coat., 12 (2019) 133–144.

[4] J.B. Tarkwa, N. Oturan, E. Acayanka, S. Laminsi, M.A. Oturan, Photo-fenton oxidation of Orange G azo dye: process optimization and mineralization mechanism, Environ. Chem. Lett., 17 (2019) 473–479.

[5] J. Saini, V. Garg, R. Gupta, Removal of Methylene Blue from aqueous solution by $Fe_3O_4@Ag/SiO_2$ nanospheres: synthesis, characterization and adsorption performance, J. Mol. Liq., 250 (2018) 413–422.

[6] U. Shanker, M. Rani, V. Jassal, Degradation of hazardous organic dyes in water by nanomaterials, Environ. Chem. Lett., 15 (2017) 623–642.

[7] Z. Eren, Ultrasound as a basic and auxiliary process for dye remediation: a review, J. Environ. Manage., 104 (2012) 127–141.

[8] P. Sharma, H. Kaur, M. Sharma, V. Sahore, A review on applicability of naturally available adsorbents for the removal of hazardous dyes from aqueous waste, Environ. Monit. Assess., 183 (2011) 151–195.

[9] W. Lang, S. Sirisansaneeyakul, L. Ngiwsara, S. Mendes, L.O. Martins, M. Okuyama, A. Kimura, Characterization of a new oxygen-insensitive azoreductase from *Brevibacillus laterosporus* TISTR1911: toward dye decolorization using a packed-bed metal affinity reactor, Bioresour. Technol., 150 (2013) 298–306.

[10] A. Spagni, S. Grilli, S. Casu, D. Mattioli, Treatment of a simulated textile wastewater containing the azo-dye reactive orange 16 in an anaerobic-biofilm anoxic–aerobic membrane bioreactor, Int. Biodeterior. Biodegrad., 64 (2010) 676–681.

[11] G. Atun, N. Ayar, A.E. Kurtoğlu, S. Ortaboy, A comparison of sorptive removal of anthraquinone and azo dyes using fly ash from single and binary solutions, J. Hazard. Mater., 371 (2019) 94–107.

[12] V. Gupta, B. Gupta, A. Rastogi, S. Agarwal, A. Nayak, A comparative investigation on adsorption performances of mesoporous activated carbon prepared from waste rubber tire and activated carbon for a hazardous azo dye—Acid Blue 113, J. Hazard. Mater., 186 (2011) 891–901.

[13] H.-Y. Shu, M.-C. Chang, C.-C. Chen, P.-E. Chen, Using resin supported nano zero-valent iron particles for decoloration of Acid Blue 113 azo dye solution, J. Hazard. Mater., 184 (2010) 499–505.

[14] J. Xun, T. Lou, J. Xing, W. Zhang, Q. Xu, J. Peng, X. Wang, Synthesis of a starch–acrylic acid–chitosan copolymer as flocculant for dye removal, J. Appl. Polym. Sci., 136 (2019) 47437.

[15] N.B.H. Abdelkader, A. Bentouami, Z. Derriche, N. Bettahar, L.C. De Menorval, Synthesis and characterization of Mg–Fe layer double hydroxides and its application on adsorption of Orange G from aqueous solution, Chem. Eng. J., 169 (2011) 231–238.

[16] D. Bassyouni, H. Hamad, E.Z. El-Ashtoukhy, N. Amin, M.A. El-Latif, Comparative performance of anodic oxidation and electrocoagulation as clean processes for electrocatalytic degradation of diazo dye Acid Brown 14 in aqueous medium, J. Hazard. Mater., 335 (2017) 178–187.

[17] M. Shestakova, M. Vinatoru, T.J. Mason, M. Sillanpää, Sonoelectrocatalytic decomposition of methylene blue using $Ti/Ta_2O_5–SnO_2$ electrodes, Ultrason. Sonochem., 23 (2015) 135–141.

[18] N. Nordin, M.A.F. Pisal, N.I.H. Razman, N.F. Jaafar, Electrochemical degradation of reactive blue 21 and synthetic textile effluent by using $Co_{47.5}/C_{47.5}$-PVC5 composite electrode, Acta Chim. Slov., 66 (2019) 284–293.

[19] M. Vakili, M. Rafatullah, B. Salamatinia, A.Z. Abdullah, M.H. Ibrahim, K.B. Tan, Z. Gholami, P. Amouzgar, Application of chitosan and its derivatives as adsorbents for dye removal from water and wastewater: a review, Carbohydr. Polym., 113 (2014) 115–130.

[20] E. Moawed, A. Abulkibash, M. El-Shahat, Synthesis and characterization of iodo polyurethane foam and its application in removing of aniline blue and crystal violet from laundry wastewater, J. Taibah Univ. Sci., 9 (2015) 80–88.

[21] G.S. Josephine, U.M. Nisha, G. Meenakshi, A. Sivasamy, Nanocrystalline semiconductor doped rare earth oxide for the photocatalytic degradation studies on Acid Blue 113: a di-azo compound under UV slurry photoreactor, Ecotoxicol. Environ. Saf., 121 (2015) 67–72.

[22] M. Pirsaheb, K. Sharafi, A. Karami, A. Dargahi, A. Ejraei, Evaluating the performance of inorganic coagulants (Poly aluminum chloride, ferrous sulfate, ferric chloride and al minum sulfate) in removing the turbidity from aqueous solutions, IJPT, 8 (2016) 13168–13181.

[23] S.D. Ashrafi, S. Rezaei, H. Forootanfar, A.H. Mahvi, M.A. Faramarzi, The enzymatic decolorization and detoxification of synthetic dyes by the laccase from a soil-isolated ascomycete, *Paraconiothyrium variabile*, Int. Biodeterior. Biodegrad., 85 (2013) 173–181.

[24] H. Cherifi, B. Fatiha, H. Salah, Kinetic studies on the adsorption of methylene blue onto vegetal fiber activated carbons, Appl. Surf. Sci., 282 (2013) 52–59.

[25] G.M. Nabil, N.M. El-Mallah, M.E. Mahmoud, Enhanced decolorization of reactive black 5 dye by active carbon sorbent-immobilized-cationic surfactant (AC-CS), Ind. Eng. Chem., 20 (2014) 994–1002.

[26] Y. Wang, L. Gai, W. Ma, H. Jiang, X. Peng, L. Zhao, Ultrasound-assisted catalytic degradation of methyl orange with $Fe_3O_4/$ polyaniline in near neutral solution, Ind. Eng. Chem. Res., 54 (2015) 2279–2289.

[27] Y. Dong, Z. Han, C. Liu, F. Du, Preparation and photocatalytic performance of Fe(III)-amidoximated PAN fiber complex for oxidative degradation of azo dye under visible light irradiation, Sci. Total Environ., 408 (2010) 2245–2253.

[28] M. Afsharnia, M. Kianmehr, H. Biglari, A. Dargahi, A. Karimi, Disinfection of dairy wastewater effluent through solar photocatalysis processes, Water Sci. Eng, 11 (2018) 214–219.

[29] M. Antonopoulou, E. Evgenidou, D. Lambropoulou, I. Konstantinou, A review on advanced oxidation processes for the removal of taste and odor compounds from aqueous media, Water Res., 53 (2014) 215–234.

[30] A. Seid-Mohammadi, G. Asgarai, Z. Ghorbanian, A. Dargahi, The removal of cephalexin antibiotic in aqueous solutions by ultrasonic waves/hydrogen peroxide/nickel oxide nanoparticles (US/H$_2$O$_2$/NiO) hybrid process, Sep. Sci. Technol., 54 (2019) 478–493.

[31] A. Zarei, H. Biglari, M. Mobini, A. Dargahi, G. Ebrahimzadeh, M.R. Narooie, E.A. Mehziri, A.R. Yari, M.J. Mohammadi, M.M. Baneshi, R. Khosravi, M. Poursadeghiyan, Disinfecting poultry slaughterhouse wastewater using copper electrodes in the electrocoagulation process, Pol. J. Environ. Stud., 27 (2018) 1907–1912.

[32] J. Wang, Y. Ding, S. Tong, Fe-Ag/GAC catalytic persulfate to degrade Acid Red 73, Sep. Purif. Technol., 184 (2017) 365–373.

[33] L. Hou, H. Zhang, X. Xue, Ultrasound enhanced heterogeneous activation of peroxydisulfate by magnetite catalyst for the degradation of tetracycline in water, Sep. Purif. Technol., 84 (2012) 147–152.

[34] S. Rodriguez, A. Santos, A. Romero, F. Vicente, Kinetic of oxidation and mineralization of priority and emerging pollutants by activated persulfate, Chem. Eng. J., 213 (2012) 225–234.

[35] M. Xu, X. Gu, S. Lu, Z. Qiu, Q. Sui, Z. Miao, X. Zang, X. Wu, Degradation of carbon tetrachloride in aqueous solution in the thermally activated persulfate system, J. Hazard. Mater., 286 (2015) 7–14.

[36] H. Zeng, S. Liu, B. Chai, D. Cao, Y. Wang, X. Zhao, Enhanced photoelectrocatalytic decomplexation of Cu–EDTA and Cu recovery by persulfate activated by UV and cathodic reduction, Environ. Sci. Technol., 50 (2016) 6459–6466.

[37] Z. Wei, F.A. Villamena, L.K. Weavers, Kinetics and mechanism of ultrasonic activation of persulfate: an in situ EPR spin trapping study, Environ. Sci. Technol., 51 (2017) 3410–3417.

[38] W.-S. Chen, C.-P. Huang, Mineralization of aniline in aqueous solution by electro-activated persulfate oxidation enhanced with ultrasound, Chem. Eng. J., 266 (2015) 279–288.

[39] M. Ahmad, A.L. Teel, R.J. Watts, Mechanism of persulfate activation by phenols, Environ. Sci. Technol., 47 (2013) 5864–5871.

[40] J. Cong, G. Wen, T. Huang, L. Deng, J. Ma, Study on enhanced ozonation degradation of para-chlorobenzoic acid by peroxymonosulfate in aqueous solution, Chem. Eng. J., 264 (2015) 399–403.

[41] S. Cotillas, M.J.M. de Vidales, J. Llanos, C. Sáez, P. Cañizares, M.A. Rodrigo, Electrolytic and electro-irradiated processes with diamond anodes for the oxidation of persistent pollutants and disinfection of urban treated wastewater, J. Hazard. Mater., 319 (2016) 93–101.

[42] O.S. Furman, A.L. Teel, R.J. Watts, Mechanism of base activation of persulfate, Environ. Sci. Technol., 44 (2010) 6423–6428.

[43] W.-S. Chen, Y.-C. Jhou, C.-P. Huang, Mineralization of dinitrotoluenes in industrial wastewater by electro-activated persulfate oxidation, Chem. Eng. J., 252 (2014) 166–172.

[44] A. Dargahi, D. Nematollahi, G. Asgari, R. Shokoohi, A. Ansari, M.R. Samarghandi, Electrodegradation of 2, 4-dichlorophenoxyacetic acid herbicide from aqueous solution using three-dimensional electrode reactor with G/β-PbO$_2$ anode: taguchi optimization and degradation mechanism determination, RSC Adv., 8 (2018) 39256–68.

[45] W. Can, H. Yao-Kun, Z. Qing, J. Min, Treatment of secondary effluent using a three-dimensional electrode system: COD removal, biotoxicity assessment, and disinfection effects, Chem. Eng. J., 243 (2014) 1–6.

[46] V. Czitrom, One-factor-at-a-time versus designed experiments, Am. Stat., 53 (1999) 126–131.

[47] R. Shokoohi, A.J. Jafari, A. Dargahi, Z. Torkshavand, Study of the efficiency of bio-filter and activated sludge (BF/AS) combined process in phenol removal from aqueous solution: determination of removing model according to response surface methodology (RSM), Desal. Water Treat., 77 (2017) 256–263.

[48] A. Almasi, A. Dargahi, M. Mohammadi, A. Azizi, A. Karami, F. Baniamerian, Z. Saeidimoghadam, Application of response surface methodology on cefixime removal from aqueous

solution by ultrasonic/photooxidation, Int. J. Pharm. Technol., 8 (2016) 16728–16736.

[49] D.C. De Moura, M.A. Quiroz, D.R. Da Silva, R. Salazar, C.A. Martínez-Huitle, Electrochemical degradation of Acid Blue 113 dye using TiO$_2$-nanotubes decorated with PbO$_2$ as anode, Environ. Nanotechnol. Monit., 5 (2016) 13–20.

[50] N.L. Pedersen, M.N. Fini, P.K. Molnar, J. Muff, Synergy of combined adsorption and electrochemical degradation of aqueous organics by granular activated carbon particulate electrodes, Sep. Purif. Technol., 208 (2019) 51–58.

[51] M.J.K. Bashir, C.J. Wei, N.C. Aun, S.S. Abu Amr, Electro persulphate oxidation for polishing of biologically treated palm oil mill effluent (POME), J. Environ. Manage., 193 (2017) 458–469.

[52] L. Bu, S. Zhou, Z. Shi, C. Bi, S. Zhu, N. Gao, Iron electrode as efficient persulfate activator for oxcarbazepine degradation: performance, mechanism, and kinetic modeling, Sep. Purif. Technol., 178 (2017) 66–74.

[53] H. Lin, Y. Li, X. Mao, H. Zhang, Electro-enhanced goethite activation of peroxydisulfate for the decolorization of Orange II at neutral pH: Efficiency, stability and mechanism, J. Taiwan Inst. Chem. Eng., 65 (2016) 390–398.

[54] A.R. Rahmani, A. Shabanloo, M. Fazlzadeh, Y. Poureshgh, H. Rezaeivahidian, Degradation of Acid Blue 113 in aqueous solutions by the electrochemical advanced oxidation in the presence of persulfate, Desal. Water Treat., 59 (2017) 202–209.

[55] A. Seid-Mohammadi, A. Shabanloo, M. Fazlzadeh, Y. Poureshgh, Degradation of Acid Blue 113 by US/H$_2$O$_2$/Fe$_{2+}$ and US/S$_2$O$_8^{2-}$/Fe$_{2+}$ processes from aqueous solutions, Desal. Water Treat., 78 (2017) 273–280.

[56] X. Wang, L. Wang, J. Li, J. Qiu, C. Cai, H. Zhang, Degradation of Acid Orange 7 by persulfate activated with zero valent iron in the presence of ultrasonic irradiation, Sep. Purif. Technol., 122 (2014) 41–46.

[57] J. Wu, H. Zhang, J. Qiu, Degradation of Acid Orange 7 in aqueous solution by a novel electro/Fe^{2+}/peroxydisulfate process, J. Hazard. Mater., 215 (2012) 138–145.

[58] N. Yang, J. Cui, L. Zhang, W. Xiao, A.N. Alshawabkeh, X. Mao, Iron electrolysis-assisted peroxymonosulfate chemical oxidation for the remediation of chlorophenol-contaminated groundwater, J. Chem. Technol. Biotechnol., 91 (2016) 938–947.

[59] D. Eeshwarasinghe, P. Loganathan, S. Vigneswaran, Simultaneous removal of polycyclic aromatic hydrocarbons and heavy metals from water using granular activated carbon, Chemosphere, 223 (2019) 616–627.

[60] S. Yang, L. Li, T. Xiao, J. Zhang, X. Shao, Reuse performance of granular-activated carbon and activated carbon fiber in catalyzed peroxymonosulfate oxidation, Environ. Technol., 38 (2016) 598–605.

[61] A. Romero, A. Santos, F. Vicente, C. González, Diuron abatement using activated persulphate: effect of pH, Fe(II) and oxidant dosage, Chem. Eng. J., 162 (2010) 257–265.

[62] A. Dargahi, A. Ansari, D. Nematollahi, G. Asgari, R. Shokoohi, M.R. Samarghandi, Parameter optimization and degradation mechanism for electrocatalytic degradation of 2,4-diclorophenoxyacetic acid (2,4-D) herbicide by lead dioxide electrodes, RSC Adv., 9 (2019) 5064–5075.

[63] M.R. Samarghandi, D. Nemattollahi, G. Asgari, R. Shokoohi, A. Ansari, A. Dargahi, Electrochemical process for 2,4-D herbicide removal from aqueous solutions using stainless steel 316 and graphite Anodes: optimization using response surface methodology, Sep. Sci. Technol., 54 (2019) 478–493.

[64] A. Mirshafiee, A. Rezaee, R.S. Mamoory, A clean production process for edible oil removal from wastewater using an electroflotation with horizontal arrangement of mesh electrodes, J. Cleaner Prod., 198 (2018) 71–79.

[65] B. Merzouk, K. Madani, A. Sekki, Using electrocoagulation–electroflotation technology to treat synthetic solution and textile wastewater, two case studies, Desalination, 250 (2010) 573–577.

[66] W.S. Chen, C.-P. Huang, Mineralization of aniline in aqueous solution by electrochemical activation of persulfate, Chemosphere, 125 (2015) 175–181.

[67] X. Zhong, S. Royer, H. Zhang, Q. Huang, L. Xiang, S. Valange, J. Barrault, Mesoporous silica iron-doped as stable and efficient heterogeneous catalyst for the degradation of CI Acid Orange 7 using sono–photo-Fenton process, Sep. Purif. Technol., 80 (2011) 163–171.

[68] S.S. Moghaddam, M.A. Moghaddam, M. Arami, Coagulation/flocculation process for dye removal using sludge from water treatment plant: optimization through response surface methodology, J. Hazard. Mater., 175 (2010) 651–657.

[69] M. Zhou, W. Wang, M. Chi, Enhancement on the simultaneous removal of nitrate and organic pollutants from groundwater by a three-dimensional bio-electrochemical reactor, Bioresour. Technol., 100 (2009) 4662–4668.

[70] M. Samarghandi, J. Mehralipour, G. Azarin, K. Godini, A. Shabanlo, Decomposition of sodium dodecylbenzene sulfonate surfactant by electro/Fe^{2+}-activated persulfate process from aqueous solutions, Global NEST J., 19 (2017) 115–121.